Albacete's model

Tomáš Herman

Faculty of Nuclear Sciences and Physical Engineering
Czech Technical University in Prague

Workshop supported by grant SVK30/19/F4

Miniworkshop difrakce a ultraperiferálních srážek
26.-27.9.2019, Děčín

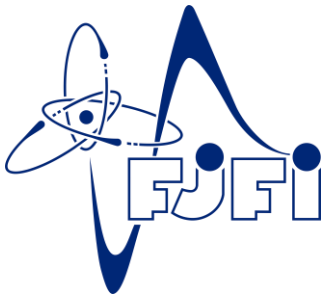

Hot spots and the hollowness of proton-proton interactions at high energies

Javier L. Albacete, Alba Soto-Ontoso

CAFPE and Departamento de Física Teórica y del Cosmos, Universidad de Granada
E-18071 Campus de Fuentenueva, Granada, Spain.

albacete@ugr.es, aontoso@ugr.es

The analysis of experimental data on the elastic proton-proton differential cross-section at collision energy $\sqrt{s}=7$ TeV measured by the TOTEM Collaboration [1] has revealed a new, intriguing feature of hadronic interactions: at high energies, the inelasticity density of the collision does not reach a maximum at zero impact parameter. Rather, peripheral collisions, where the effective geometric overlap of the colliding protons is smaller, are more inelastic or, equivalently, are more effective in the production of secondary particles than central ones. This phenomenon, not observed before at lower collision energies, has been referred to as *hollowness* [2] or *grayness* [3–5] of proton-proton collisions by the authors of the first analyses where it was identified.

be described below, confirms that the inelasticity density of the collision

$$G_{\rm in}(s,\vec{b}) \equiv \frac{{\rm d}^2\sigma_{\rm inel}}{{\rm d}^2 b} = 2{\rm Im}\widetilde{T}_{\rm el}(s,\vec{b}) - |\widetilde{T}_{\rm el}(s,\vec{b})|^2 \,, \qquad (1)$$

where $\widetilde{T}_{\rm el}(s,\vec{b})$ is the scattering amplitude in the impact parameter representation, reaches a maximum at $b \neq 0$ for a collision energy $\sqrt{s}=7$ TeV, as shown in Fig. 1.

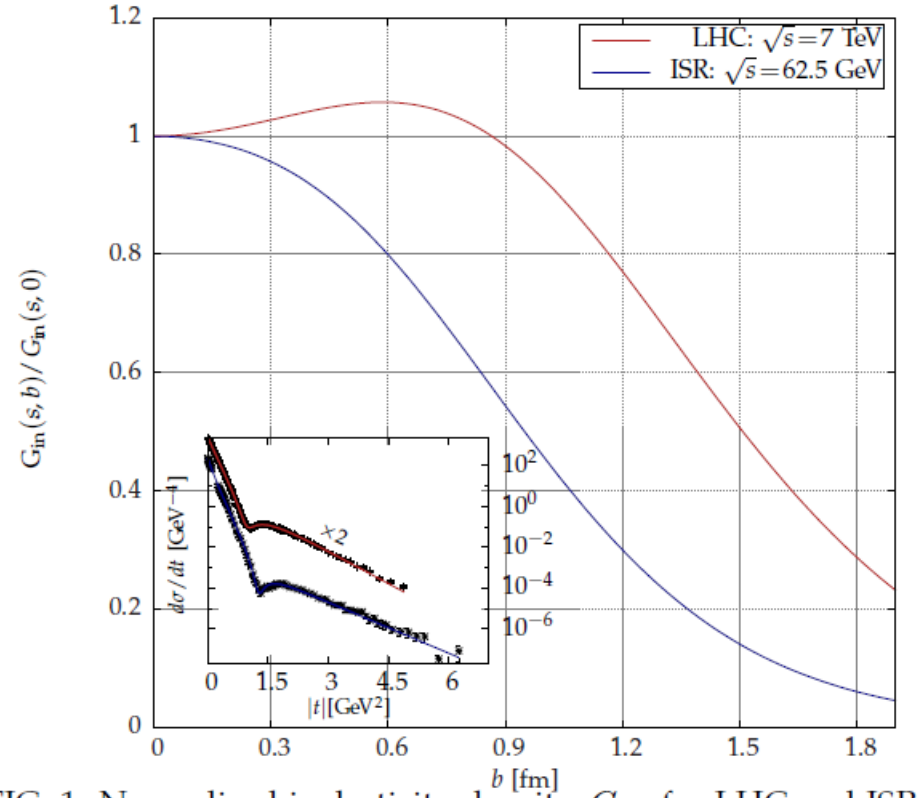

FIG. 1: Normalised inelasticity density, $G_{\rm in}$, for LHC and ISR energies as a function of the impact parameter. Sub-pannel: fits to ${\rm d}\sigma_{\rm el}/{\rm d}t$ data.

The *hollowness* effect challenges the standard geometric interpretations of proton-proton collisions. In particular, it precludes models where the scattering amplitude is built in terms of a positive dependence on the convolution of the density profiles of the two colliding protons. Indeed, it can be shown that the inelasticity

The idea that the gluon content of the proton is concentrated in domains of small radius R_{hs}, much smaller than the proton electromagnetic radius that controls the valence quark distribution $R_{hs} \ll R_p$, is strongly supported by theoretical and phenomenological arguments.

and simply assume that hot spots are adequate degrees of freedom to discuss inclusive proton-proton scattering at high energies. Our main assumption about their dynamical properties is that collisions between hot spots are fully absorptive over distances smaller than their radius, R_{hs}. Hence, in our effective description, hot spots appear as small black disks of average radius R_{hs}. We also assume implicitly that their ultimate dynamical origin is correlated to the valence partons, since we model the proton as composed of $N_{hs}=3$ hot spots.

representation. We describe pp interactions as a collision of two systems, each one composed of three hot spots. According to the Glauber model, the natural framework

momentum. Next, we implement repulsive short-range correlations between all pairs of hot spots controlled by an effective repulsive core $r_c \equiv R/\mu$. In the limit $\mu \to \infty$ we recover the uncorrelated case. While we have no clear dynamical justification for these correlations, their main role in our calculation is to enforce a larger transverse separation between hot spots with respect to the completely uncorrelated case. Indeed, all realistic mod-

where R is the average radius of the d distribution. It product of three uncorrelated probability distributions for a single hot spot, $d(\vec{s}_i)$. In order to facilitate a full an-

mentally. It should be noted that all the energy dependence in our model has been left implicit so far. As discussed below, it is encoded in the transverse growth of the hot spot radius R_{hs} with increasing collision energy,

In order to prove that our model actually accounts for the onset of hollowness effect at high energies, we scan the parameter space looking for the presence of a dip of the inelasticity density at zero impact parameter and a monotonically decreasing scattering amplitude, as dic-

A first, important result is that it is not possible to obtain a growing behaviour of $G_{\rm in}(s,b)$ at zero impact parameter in the absence of non-trivial correlations, i.e for $\mu \to \infty$ in Eq. 7 or, equivalently for zero correlation distances $r_c = 0$. Indeed, in this case the full calculation of

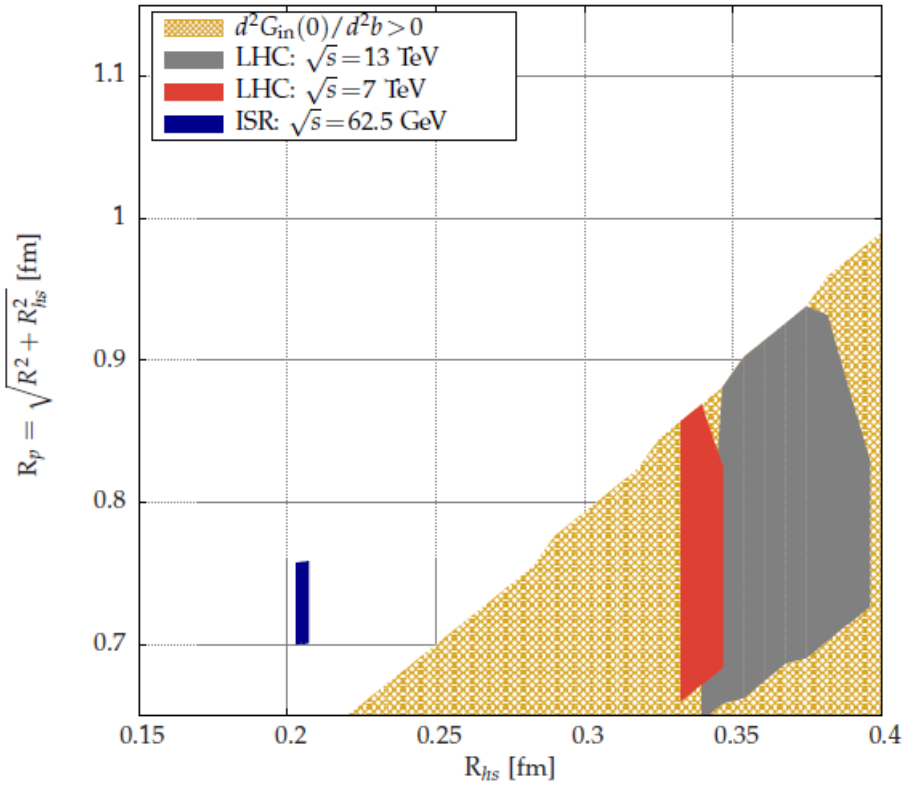

We hence conclude that the main dynamical process underlying the onset of the hollowness effect is the transverse diffusion or growth of the hot spots with increasing collision energy, which is the main result of this work. Further, the measured growth of the total proton-

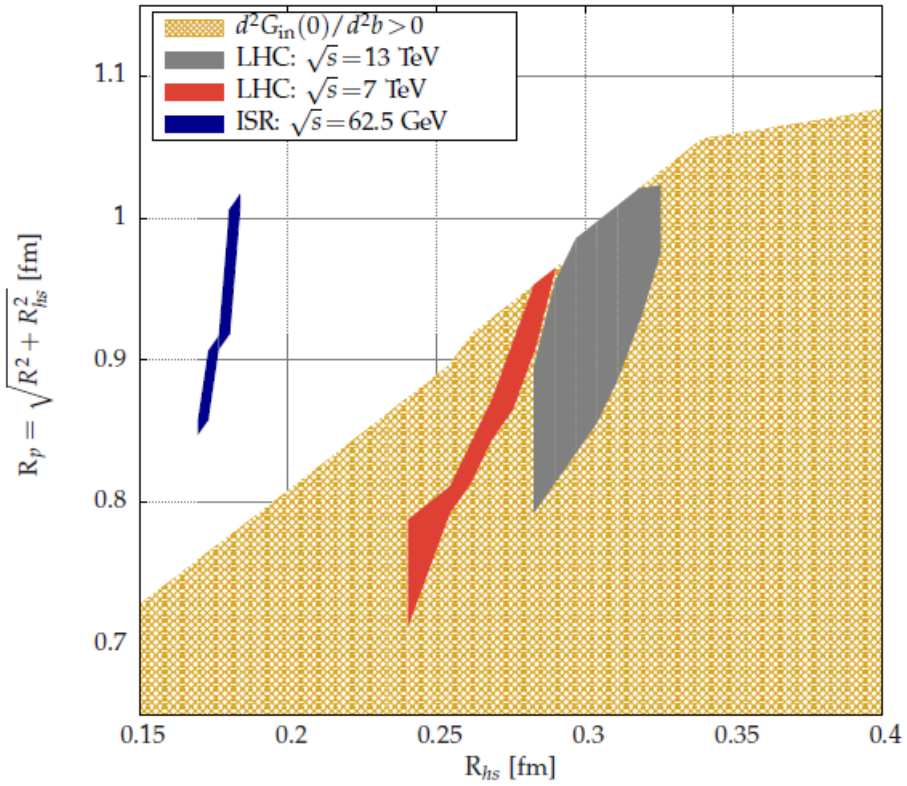

FIG. 3: Hollowness region (filled-dashed) and phenomenologically compatible regions with LHC and ISR data in the (R_p, R_{hs})-plane for $r_c=0.3$ (top) and 0.5 fm (bottom).

Summary

In summary, we propose that the explanation to the rather counterintuitive hollowness effect –whereby proton peripheral collisions are more destructive than central ones at high energies– lies in the interplay between the different internal scales of the proton: proton radius, hot spot radius and transverse correlation length. The relative enhancement of the destructive interference terms in the multiple scattering series –known as *shadowing* corrections– induced by non-trivial probability densities for the hot spots transverse positions and the swelling hot spots radius with increasing energy yield the observed depletion of the inelasticity density in central collisions. These effects may have observable consequences in other sets of experimental data on proton collisions. Arguably, they could impact significantly the interpretation of data specially sensitive to the initial collision geometry, like the correlation and flow analysis of proton-proton collisions and the possible production of small drops of Quark Gluon Plasma in such collisions, a highly debated topic nowadays.

Correlated wounded hot spots in proton-proton interactions

Javier L. Albacete,[1,*] Hannah Petersen,[2,3,4,†] and Alba Soto-Ontoso[1,2,‡]

[1]*CAFPE and Departamento de Física Teórica y del Cosmos, Universidad de Granada, E-18071 Campus de Fuentenueva, Granada, Spain.*

[2]*Frankfurt Institute for Advanced Studies, Ruth-Moufang-Strasse 1, 60438 Frankfurt am Main, Germany.*

[3]*Institute for Theoretical Physics, Goethe University,Max-von-Laue-Strasse 1, 60438 Frankfurt am Main, Germany.*

[4]*GSI Helmholtzzentrum für Schwerionenforschung, Planckstr. 1, 64291 Darmstadt, Germany.*

plasma (QGP) [1]. One of the most important observables supporting the discovery of the QGP is the high value of the elliptic flow v_2. It quantifies how the ini-

2.76, 5.02 TeV [2, 3]. Originally, elementary collisions such as proton-proton (pp) or proton-nucleus (pA) were supposed to provide the binary collisions/cold nuclear matter baseline for heavy ion collisions. However, the analyses of particle correlations in very high multiplicity pp collisions at the LHC at $\sqrt{s}=7$ TeV have revealed striking similarities to the AA case. Suggestive signals of collective behavior such as non-negligible elliptic flow

To compute the spatial eccentricities and have access to event-by-event fluctuations we have developed a Monte-Carlo Glauber event generator inspired by [30,

First of all, the impact parameter of the collision is chosen randomly from the distribution

$$\mathrm{d}N_{\mathrm{ev}}/\mathrm{d}b \propto b \tag{1}$$

up to $b_{\mathrm{max}} = 2$ fm $\gtrsim 2R_p$. In our picture, the im-

We describe pp interactions as a collision of two systems, each one composed of three hot spots. The posi-

and refer to them as *wounded* [35, 36], if they have suffered at least one collision. Thus, the maximum num-

Eq. 2, we have considered two extreme scenarios: the uncorrelated case labeled as $r_c = 0$ and a repulsive core of 0.4 fm labeled as $r_c = 0.4$. Being the main goal of this work to explore the net effect of correlations we have considered a third situation, $r_c = 0, nc$, in which we set the repulsive distance to 0 but choose the values of $\{R_{hs}, R, \rho_{hs}\}$ as in the $r_c = 0.4$ case, not reproducing though the experimental values of σ_{tot} and ρ. The main reason to consider this additional possibility is that differences between the results of $r_c = 0.4$ and $r_c = 0, nc$ are then only attributable to the presence of short-range repulsive correlations as the rest of the parameters remain identical. However for the same values of $\{R_{hs}, R, r_c, \rho_{hs}\}$ the hot spots of the correlated distribution have a larger mean transverse position, $\langle s_1 \rangle$, defined as

$$\langle s_1 \rangle = \int s_1 \mathrm{d}\vec{s}_1 \mathrm{d}\vec{s}_2 \mathrm{d}\vec{s}_3 D(\vec{s}_1, \vec{s}_2, \vec{s}_3) \qquad (4)$$

where $D(\vec{s}_1, \vec{s}_2, \vec{s}_3)$ is given by Eq. 2, than in the uncorrelated case. In order to avoid this artificial swelling we have included one last scenario, labeled as "$\langle s_1 \rangle$ fixed", in which $\{R_{hs}, r_c, \rho_{hs}\}$ are the same as in the $r_c = 0.4$ case but R is chosen to reproduce the $\langle s_1 \rangle$ of the correlated distribution. The values of R for this case are shown in

Essentially, entropy deposition is directly related to the number of charged particles produced in pp collisions.

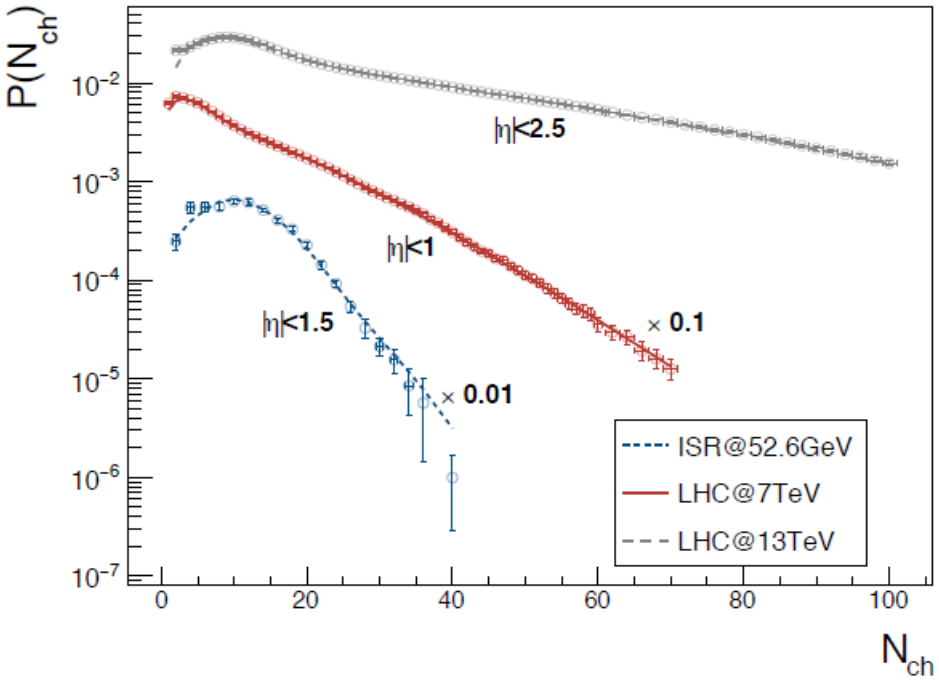

Figure 1. Fit to the charged particle multiplicity distributions for different collision energies in the wounded hot spot model, Eqs. 7-8. The experimental data from top to bottom is taken from: ATLAS Collaboration [42], ALICE Collaboration [43] and ISR [44]. Note that each experiment has a different rapidity acceptance window, η, that influences the shape of the data. Also, the ALICE (red) and ISR (blue) curves are multiplied by 0.1 and 0.01 respectively.

Within the current context, the main purpose of an accurate description of the charged hadron multiplicity distribution is to provide phenomenological guidance to a non-measurable quantity, the shape of the entropy distribution. In general, the negative binomial distribu-

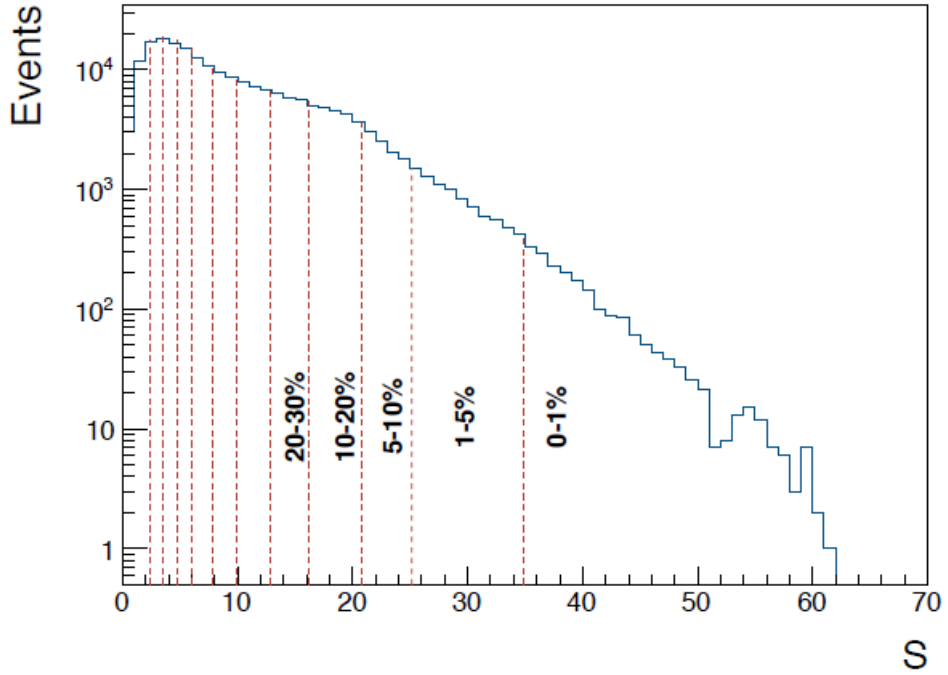

Figure 2. The histogram of the integrated entropy deposition for the $r_c = 0.4$ fm case at $\sqrt{s} = 7$ TeV. Vertical red lines labelled by black numbers define centrality classes as fractions of the total number of events.

A quantitative measurement of the initial anisotropy of the geometry in a collision is given by the spatial eccentricities that are defined as

$$\varepsilon_n = \frac{\sqrt{\langle \sum_{i=1}^{N_w} r_i^n \cos(n\phi_i)\rangle^2 + \langle \sum_{i=1}^{N_w} r_i^n \sin(n\phi_i)\rangle^2}}{\langle \sum_{i=1}^{N_w} r_i^n \rangle} \quad (5)$$

where the sum runs over all wounded hot spots. The po-

We present our results in two different cases: all the events are selected (minimum bias) and only the events on the 0-1% centrality class (ultra-central collisions) as

We begin our analysis by computing the average number of wounded hot spots in pp collisions as a function of the impact parameter b for the four different scenarios introduced above. The results are shown in Fig. 3. We note that the qualitative behavior of the impact parameter dependence of $\langle N_w \rangle$ is not affected by the inclusion of correlations. For instance, the num-

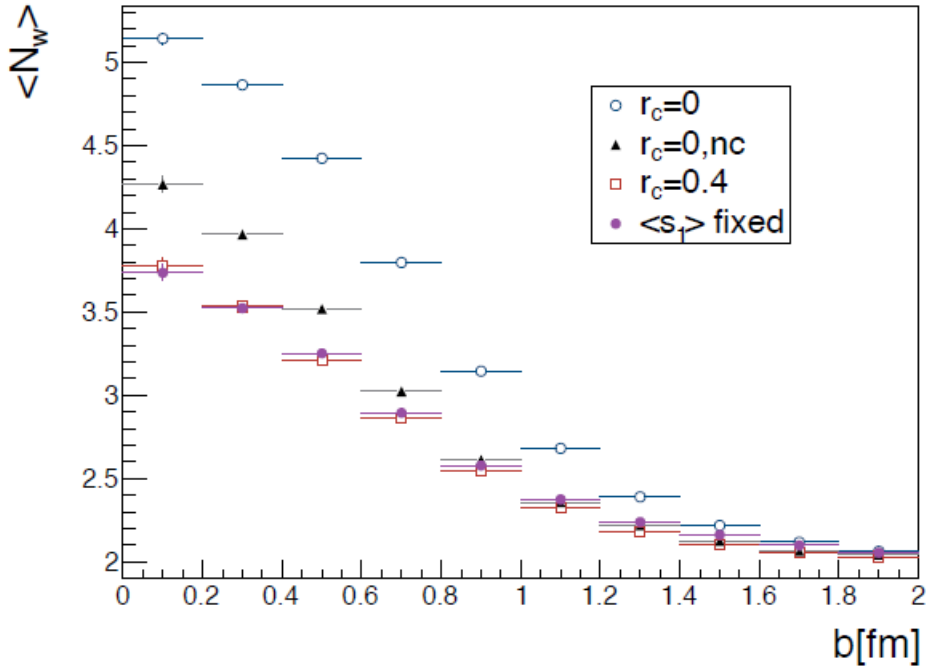

Figure 3. Average number of wounded hot spots for different impact parameter bins of the collision. The horizontal lines indicate the width of the bins.

The main result of this Section is shown in Fig. 5: the eccentricity, ε_2, is reduced in the correlated scenario compared to the rest of the cases including the one with $\langle s_1 \rangle$ fixed. We hence conclude that the probability of

having smaller values of the eccentricity in a proton-proton interaction is increased when repulsive short-range correlations are included. In essence the eccen-

smaller eccentricity) in the correlated scenario. However, all cases exhibit a broad probability distribution of ε_2 due to the highly fluctuating nature of the system. In addition, the effect of correlations between the

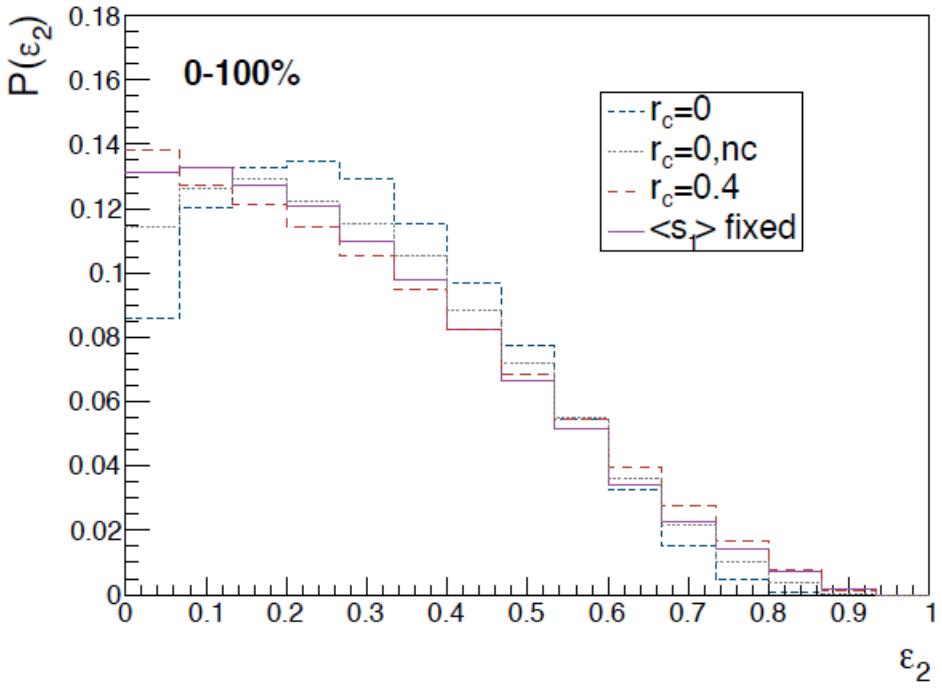

Figure 5. Probability distribution of the eccentricity, ε_2, for $r_c = 0$ (blue short-dashed line), $r_c = 0.4$ fm (red long-dashed line), $r_c = 0, nc$ (grey dotted line) and $\langle s_1 \rangle$ fixed (purple solid line).

To conclude this Section we show in Fig. 6 the probability distribution for the triangularity, $\mathcal{P}(\varepsilon_3)$. The ori-

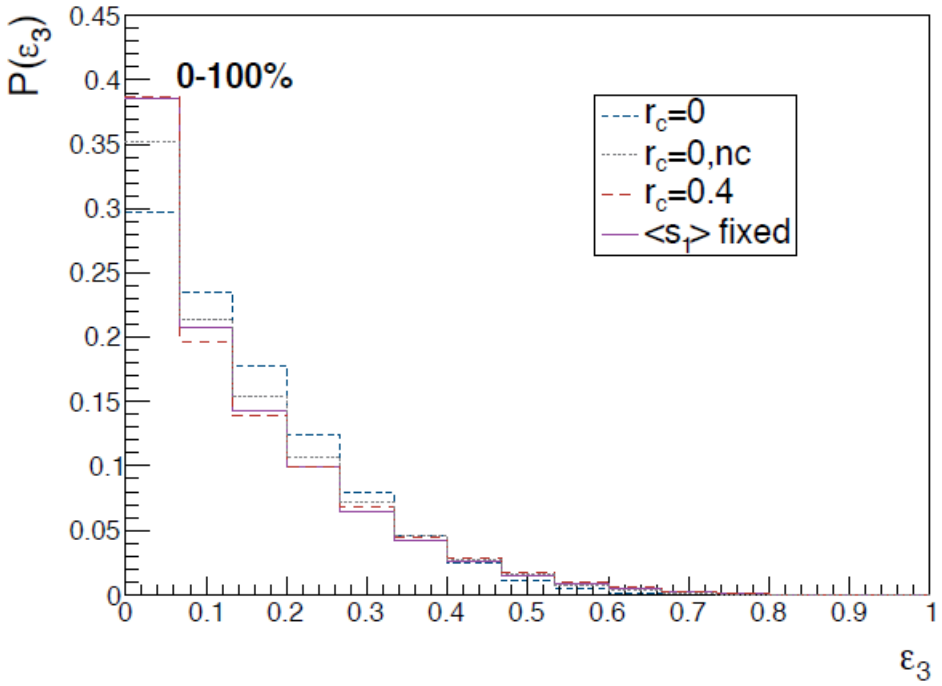

Figure 6. Probability distribution of the triangularity, ε_3, for $r_c = 0$ (blue short-dashed line), $r_c = 0.4$ fm (red long-dashed line), $r_c = 0, nc$ (grey dotted line) and $\langle s_1 \rangle$ fixed (purple solid line).

we observe how the probability distributions $\mathcal{P}(\varepsilon_{2,3})$ are shifted towards larger values when selecting ultra-central events both in the uncorrelated and correlated scenarios. Next, focusing on the role of correlated constituents in this high-entropy context we observe that it turns out to favor higher values of ε_2 and ε_3 when compared to the uncorrelated scenario. Thus, we find that the consequence of having correlated constituents inside the proton is the opposite in ultra-central collisions than in minimum bias. To sum up, in the 0–1% centrality class the net effect of correlations is to increase the probability of having larger values of $\varepsilon_{2,3}$ whereas in the minimum bias case this probability is diminished.

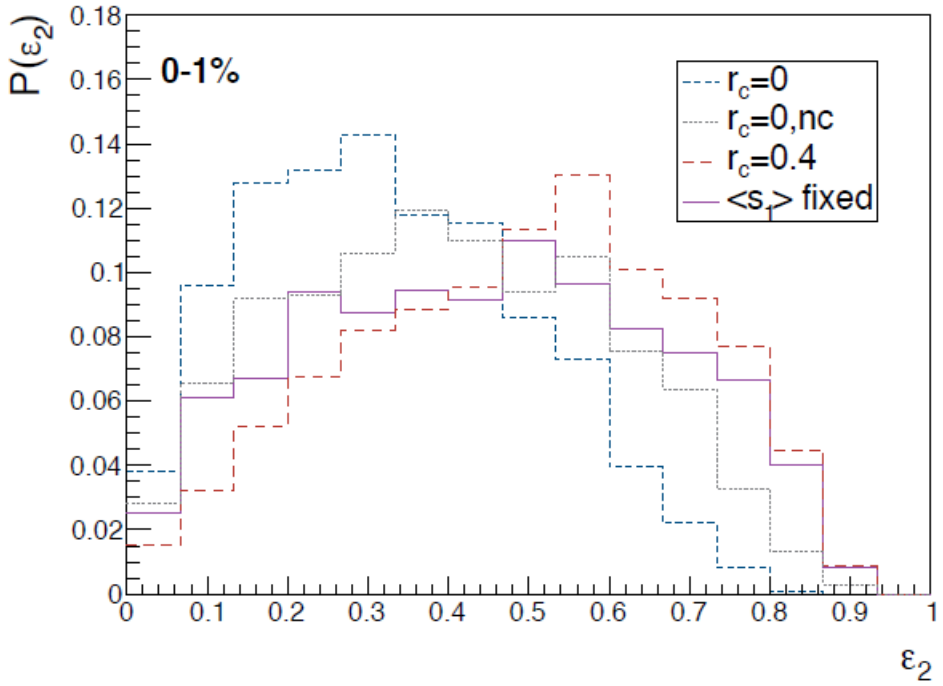

Figure 7. Probability distribution of the eccentricity, ε_2, for $r_c = 0$ (blue short-dashed line), $r_c = 0.4$ fm (red long-dashed line), $r_c = 0, nc$ (grey dotted line) and $\langle s_1 \rangle$ fixed (purple solid line) after selecting the 1% most *entropic* events.

central events than in minimum bias. Thus, we conclude that the net effect of correlated constituents is larger in ultra-central collisions.

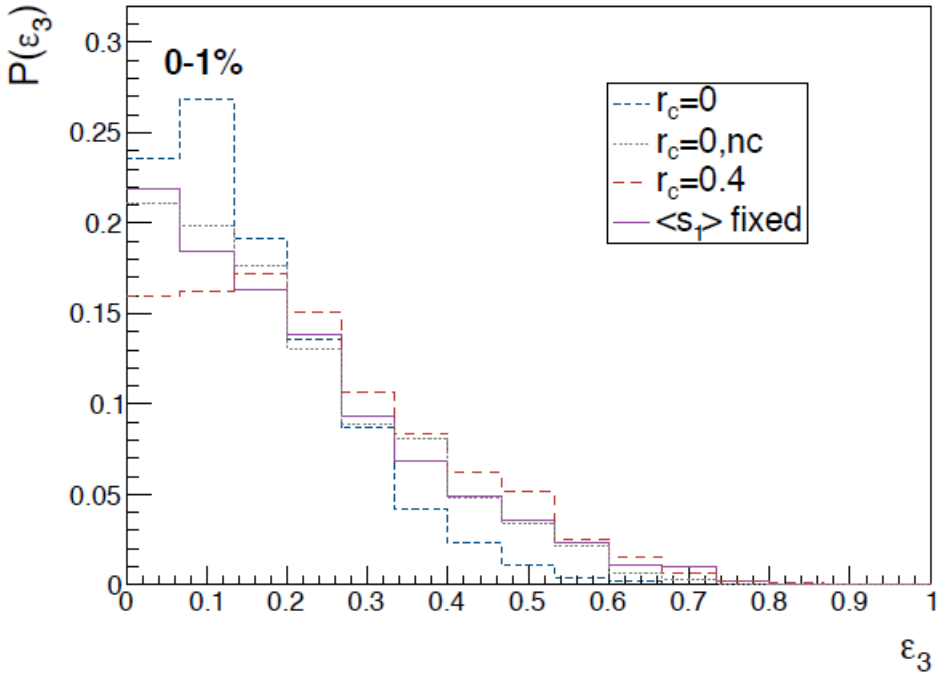

Figure 8. Probability distribution of the triangularity, ε_3, for $r_c = 0$ (blue short-dashed line), $r_c = 0.4$ fm (red long-dashed line), $r_c = 0, nc$ (grey dotted line) and $\langle s_1 \rangle$ fixed (purple solid line) after selecting the 1% most *entropic* events.

that, in agreement with [12], we find moderate variations in the mean number of wounded hot spots as the energy increases. Indeed, for the $r_c = 0.4$ case we obtain $\overline{N}_w = 2.3,\ 2.74,\ 2.75$ at $\sqrt{s} = 52.6$ GeV, 7 TeV and 13 TeV respectively. The rising behavior of $\overline{N}_w$ with increasing collision energy can be directly attributed to the growth of R_{hs} as depicted in Table I. In other words, in a

Fig. 11 is to show that there are no significant differences in the values of $\langle \varepsilon_2 \rangle$ and $\langle \varepsilon_3 \rangle$ for different collision energies. The fact that the spatial eccentricities do not drasti-

Summary

production for future work. Essentially, the presence of correlations affect the geometry of the collision leading to variations in the basic elements of the Monte-Carlo Glauber model such as the mean number of wounded hot spots or their radial distribution in the transverse plane. In particular, we show that these correlations may produce a notorious reduction both of the eccentricity and on the triangularity in minimum bias events. However, when a cut in the entropy deposition is applied to select the 1% of most entropic events the effect of correlations is the opposite: larger eccentricities and triangularities are expected in the correlated scenario than in the uncorrelated one in ultra-central collisions. We attribute this result to the fact that in our model the entropy deposition is computed as an incoherent superposition (see Eq. 12) of the individual contributions of each wounded hot spot, the more wounded hot spots the larger the entropy deposited. Then, upon imposing this high-entropy cut we are implicitly selecting events with a large number of wounded hot spots. In these configurations the spatial correlations increase the values of ε_2 and ε_3 with respect to the uncorrelated cases. In addition to the effect of correlations on the properties of the initial state we have explored their energy dependence from ISR to the LHC finding small deviations in the values of ε_2 and ε_3. The results presented in this article

Thank you for your attention!

Backup